


## Theory of the Loschmidt echo and dynamical quantum phase transitions in disordered Fermi systems

Tuomas I. Vanhala  and Teemu Ojanen 

*Computational Physics Laboratory, Physics Unit, Faculty of Engineering and Natural Sciences, Tampere University,  
P.O. Box 692, FI-33014 Tampere, Finland  
and Helsinki Institute of Physics P.O. Box 64, FI-00014, Finland*

 (Received 24 November 2022; revised 11 August 2023; accepted 16 August 2023; published 11 September 2023)

In this work we develop the theory of the Loschmidt echo and dynamical phase transitions in noninteracting strongly disordered Fermi systems after a quench. In finite systems the Loschmidt echo displays zeros in the complex time plane that depend on the random potential realization. Remarkably, the zeros coalesce to form a 2D manifold in the thermodynamic limit, atypical for 1D systems, crossing the real axis at a sharply defined critical time. We show that this dynamical phase transition can be understood as a transition in the distribution function of the smallest absolute value of the eigenvalues of the Loschmidt matrix and develop a finite-size scaling theory. Contrary to expectations, the notion of dynamical phase transitions in disordered systems becomes decoupled from the equilibrium Anderson localization transition. Our results highlight the striking qualitative differences of quench dynamics in disordered and nondisordered many-fermion systems.

DOI: [10.1103/PhysRevResearch.5.033178](https://doi.org/10.1103/PhysRevResearch.5.033178)

### I. INTRODUCTION

Equilibrium statistical physics is one of the most general theories in natural sciences—it has been successfully applied to a remarkably wide variety of systems between the smallest and the largest scales in the universe. Only recently, the advent of modern quantum simulators and digital quantum computers has enabled a detailed experimental access to coherent far-from-equilibrium quantum evolution [1–10]. One aspect of this that has recently stimulated enormous interest is the possibility for nonanalytic behavior generated by a sudden quench. This phenomenon, often discussed in terms of a many-body Loschmidt echo, has close analogies with equilibrium phase transitions which give rise to well-known nonanalytic properties as a function of the control parameter driving the transition. In contrast, a so-called dynamical quantum phase transition, taking place at a critical time  $t_c$ , signifies a vanishing Loschmidt echo and an abrupt change in the temporal evolution [11]. The possibility of nonanalytic evolution is in itself intriguing, however, the formal analogy with equilibrium criticality has launched a search for possible universality in far-from-equilibrium systems [11,12].

In this work we establish the theory of Loschmidt echo and dynamical quantum phase transitions in noninteracting disordered many-fermion systems. We discover that the singular dynamics of disordered Fermi systems constitute a radical departure from the previously studied many-body quenches. We find that (i) the temporal evolution of the studied sys-

tem after a generic quench is accompanied by a vanishing Loschmidt echo after a finite time, (ii) the critical time, when the Loschmidt echo vanishes, becomes a deterministic nonfluctuating quantity in the thermodynamic limit, (iii) the Loschmidt echo remains strictly zero after the critical time, and (iv) the qualitative behavior of the Loschmidt echo does not depend on whether the quench crosses the equilibrium Anderson localization critical point or not. Many insights on dynamical phase transitions have been obtained from free-fermion systems and subsequently confirmed in a number of strongly correlated systems. Thus, our present work provides a baseline to understand singular dynamics of even more complex disordered systems in the future.

### II. PROTOTYPE MODEL AND QUENCH PROTOCOL

We consider sudden quenches between two generic, noninteracting fermionic Hamiltonians  $H_0$  and  $H_1$ . The initial state  $|\psi\rangle$  of the system at time  $t = 0$  is taken to be an  $N_p$ -particle eigenstate of  $H_0$ , which is then propagated by  $H_1$ . Since both  $H_0$  and  $H_1$  are noninteracting, the state is a Slater determinant for all times. Collecting the  $N_p$  occupied orbitals in the initial state as columns of the matrix  $V$ , the evolved state  $|\psi(t)\rangle$  is represented by a Slater determinant of the columns of  $V(t) = \exp(-itH_1)V$ , while the associated Loschmidt echo is given by [13]

$$Z(t) = \langle \psi | \psi(t) \rangle = \det(M(t)), \quad (1)$$

where the Loschmidt matrix  $M(t)$  is defined as  $M(t) = V^\dagger V(t)$ . It is convenient to consider the echo in the eigenbasis of  $H_1$  represented as  $H_1 = U_1 E_1 U_1^\dagger$ , where columns of  $U$  are the eigenstates of  $H_1$  and  $E_1$  is a diagonal matrix of the

*Published by the American Physical Society under the terms of the Creative Commons Attribution 4.0 International license. Further distribution of this work must maintain attribution to the author(s) and the published article's title, journal citation, and DOI.*

eigenenergies. The matrix  $M(t)$  can be written as

$$M(t) = V^\dagger U_1 \exp(-itE_1) U_1^\dagger V, \quad (2)$$

and the echo is determined by the basis change matrix  $V^\dagger U_1$  and the distribution of the energies  $E_1$ . We note that the time  $t$  is taken to be a complex variable in general, and the Loschmidt echo of a finite system is an analytic function on the whole complex plane [11].

As a prototype we consider a 1D Anderson model with a second quantized Hamiltonian of the form

$$H = J \sum_{i=1}^L (c_i^\dagger c_{i+1} + c_{i+1}^\dagger c_i) + \sum_{i=1}^L h_i c_i^\dagger c_i. \quad (3)$$

We call this the microscopic model as opposed to the random matrix model introduced below. It is instructive to first consider the extreme quench where the initial Hamiltonian  $H_0$  is free from disorder  $h_i = 0$ ,  $J = 1$  while the final Hamiltonian  $H_1$  has no hopping  $J = 0$  and  $h_i$  are drawn from a uniform distribution in the interval  $[-h/2, h/2]$ . We quench from an eigenstate of  $H_0$ , randomly choosing  $N_p$  single-particle states to be occupied, and propagate with the Hamiltonian  $H_1$ , whose spectrum is just given by the  $h_i$ . We always consider half-filling,  $N_p = L/2$ .

It is revealing to compare the microscopic model with a random matrix model where the initial Hamiltonian  $H_0 = U_0 E_0 U_0^\dagger$  is drawn from the Gaussian unitary ensemble (GUE). It then makes no difference what the eigenstates of  $H_1$  are, as  $U_0$  is distributed according to the circular unitary ensemble (CUE) and, by the invariance of the Haar measure, so is the overlap matrix  $U_0^\dagger U_1$  regardless of what  $U_1$  is. The matrix  $V^\dagger U_1$  is thus just a randomly chosen collection of row vectors from a CUE random matrix regardless of  $U_1$ . We still assume that the energies  $E_1$  are the same as in the microscopic model, i.e., uniformly distributed in the interval  $[-h/2, h/2]$ . In the following we call this model the GUE model.

Dynamical phase transitions are revealed by the zeros of  $Z(t)$ , termed the Loschmidt zeros, in the complex  $t$  plane. A dynamical phase transition takes place at a critical time  $t_c$ , where the manifold of zeros intersects the real time axis. However, first we explore the Loschmidt echo by following the evolution of the eigenvalues of  $M(t)$  and plotting them in the upper row of Fig. 1. As  $Z(t)$  is the determinant of  $M(t)$ , zeros of  $Z(t)$  appear at points  $t$  where  $M(t)$  has eigenvalue zero. We notice that the spectrum of  $M(t)$  falls within a well-defined, bounded region at all times. After the appearance of the first zero eigenvalue, the spectrum of  $M(t)$  encapsulates the origin at all times. This signifies a type of singular many-body dynamics where the Loschmidt echo vanishes for all times after first reaching zero and the only singularity of the rate function is at the critical time, similarly to the quench within the massless phase in the 2D Kitaev model [14]. Here we observe a certain universality, as the microscopic model and the GUE model produce essentially the same eigenvalue distribution.

We can now confirm the nature of the DQPT also by directly looking at the Loschmidt zeros located using the cumulant method developed in Ref. [15]. We discuss the specialization of the method to the noninteracting case in Appendix B. In this case, as also clarified below, the

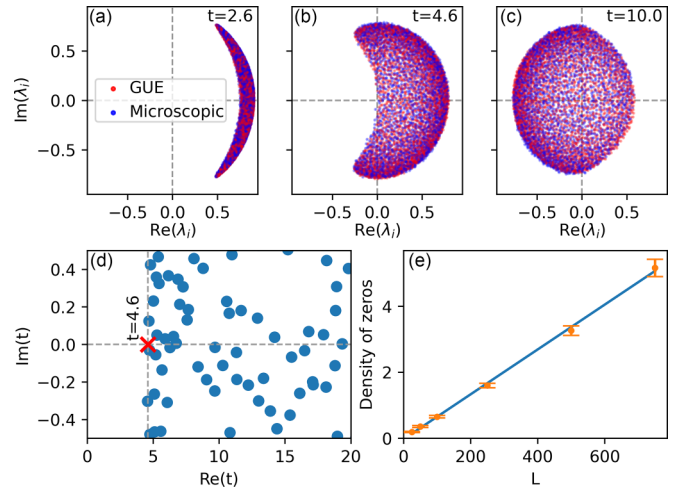


FIG. 1. Dynamical phase transition following a very strong sudden quench. The energies  $h_i$  are distributed in the interval  $[-\frac{1}{2}, \frac{1}{2}]$ . (a)–(c) Eigenvalues of the  $M(t)$ -matrix for two different models, the GUE model and the microscopic model, which exhibit remarkable similarity. The dynamical phase transition occurs at the point  $t = t_c$  where the boundary of the eigenvalue distribution crosses the origin. The system size is  $L = 5000$ . (d) Loschmidt zeros for a single realization of the microscopic model of size  $L = 500$ . The red cross marks the dynamical phase transition point where the real axis intersects the boundary of the area with a finite zero-density. (e) Scaling of the average density of zeros with system size  $L$  in the region  $15 < \text{Re}(t) < 25$ ,  $|\text{Im}(t)| < 0.2$  for the microscopic model. The datapoints were calculated with 100 realizations of the random potential for each  $L$  and the line is a linear regression.

Loschmidt zeros are organized as a 2D manifold. As seen in the lower left panel of Fig. 1, the zeros indeed cross the real time axis at the time  $t_c$  which coincides with the first appearance of zero eigenvalue of  $M(t)$ . The density of zeros in the region  $t > t_c$  increases proportionally to  $L$ , which we also verify numerically in Fig. 1(e). The zeros thus form a two-dimensional manifold previously found in two-dimensional models [14], while one-dimensional models typically display lines of zeros [11]. Here, however, the zero manifold is two-dimensional for both the 1D microscopic model and for the random matrix model where the propagating Hamiltonian only enters through its eigenenergies, which are not directly related to its dimensionality.

### III. EIGENVALUE PHASE TRANSITION AND SCALING THEORY

In the case of extreme quenches between clean and non-hopping states discussed above, the eigenvalue distribution of  $M(t)$  appears to have a sharp boundary and the critical time  $t_c$  is easily located by simply following the evolution of eigenvalues in the complex plane. However, for generic quenches this is not the case, as the boundary of the eigenvalue distribution in the thermodynamic limit may be difficult to determine from the finite set of eigenvalues calculated for some attainable system size  $L$ . Indeed, the question remains whether such a sharp boundary generally exists even in the thermodynamic limit. This is demonstrated

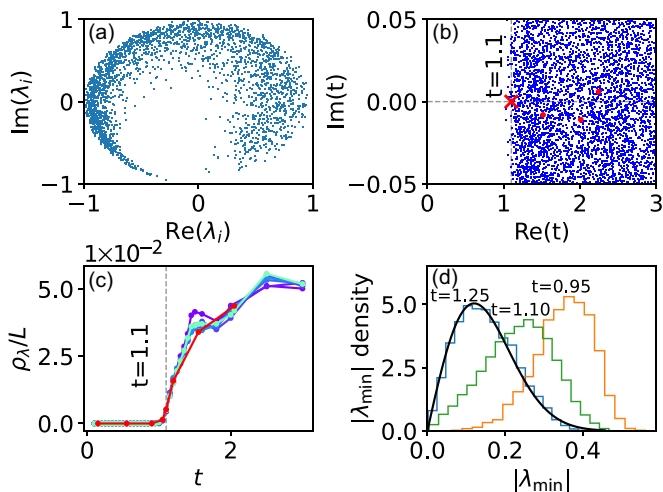


FIG. 2. Quenching from the ground state of the ( $h = 0, J = 1$ ) system to the ( $h = 5, J = 1$ ) system. (a) Eigenvalues of  $M(t)$  for a single potential realization in a system of size  $L = 5000$  at the approximate critical time  $t = 1.1$ . (b) Combined Loschmidt zeros for system size  $L = 500$  and  $N_s = 1401$  potential realizations. The red dots highlight the zeros for one realization, showing their rarity. The red cross indicates the dynamical phase transition. (c) The density of eigenvalues of  $M(t)$  within a small disk of radius 0.05 around the origin averaged over a large number of potential realizations. The color coding for system sizes and the sample sizes are as in Fig. 3. (d) Histogram of  $N_s = 10000$  samples of  $|\lambda_{\min}|$  for different times in the  $L = 500$  system. The black line is a Rayleigh distribution fitted to the data at  $t = 1.25$ .

in Fig. 2(a) for a quench starting from the ground state of Hamiltonian (3) at parameters ( $h = 0, J = 1$ ) and propagated with ( $h = 5, J = 1$ ).

To gain a quantitative understanding of the dynamical phase transitions in such cases, we consider ensembles of quenches for different realizations of the random potential. In Fig. 2(b) we plot the combined Loschmidt zeros for 100 systems of length  $L = 500$ . Although the zeros for a single system are very sparse, the ensemble reveals a sharp boundary where the zeros appear. From the viewpoint of the eigenvalues of  $M(t)$ , the same boundary is found by inspecting the density  $\rho_\lambda$  of eigenvalues close to the origin averaged over the ensemble [see Fig. 2(c)]. But is this sharp transition a property of the ensemble, or a property of an individual quench in the thermodynamic limit? If we could increase the system size sufficiently, then would we obtain a sharp nonfluctuating critical time for an individual quench? To answer this question, we propose to study the distribution of  $|\lambda_{\min}|$ , where  $\lambda_{\min}$  is an eigenvalue of  $M(t)$  with the smallest absolute value. This is related to, although not the same as the smallest singular value of  $M(t)$ , which has been studied in classical random matrix ensembles [16,17].

Suppose now that a sharp boundary for the eigenvalue distribution of  $M(t)$  exists in the thermodynamic limit. Then, for  $t < t_c$ , the distribution of  $|\lambda_{\min}|$  should become increasingly narrow with increasing  $L$ , and its mean  $\langle |\lambda_{\min}| \rangle$  should approach a finite value corresponding to the distance from the origin to the boundary of the eigenvalue distribution. For times  $t > t_c$ , however, both the mean and the standard

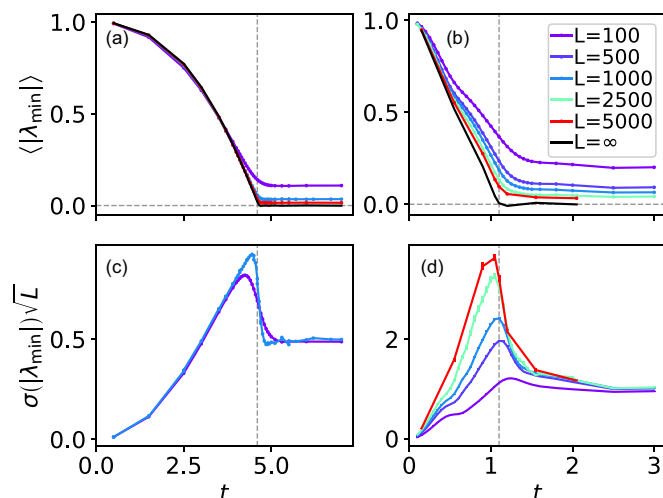


FIG. 3. Mean and scaled standard deviation of the distribution of  $|\lambda_{\min}|$  calculated for an ensemble of  $N_s = 10000$  systems for  $L \leq 500$  and  $N_s = 1000$  for  $L \geq 1000$ . Panels a and c show the quench of the microscopic model also considered in Fig. 1, while panels (b) and (d) show the quench from the *ground state* of Hamiltonian 3 at  $h = 0, J = 1$  propagated with the same Hamiltonian at parameters  $h = 5, J = 1$ . Black lines are calculated by a linear extrapolation in  $1/\sqrt{L}$ . The vertical dashed lines show the estimated critical time.

deviation  $\sigma(|\lambda_{\min}|)$  of the distribution should scale to zero with increasing  $L$ . If we assume that the eigenvalues of  $M(t)$  in the vicinity of the origin are drawn independently from some smooth distribution with local density  $\rho_\lambda$ , we find that the distribution of  $|\lambda_{\min}|$  converges to the Rayleigh form

$$f(|\lambda_{\min}|) = 2\pi |\lambda_{\min}| \rho_\lambda \exp(-\pi \rho_\lambda |\lambda_{\min}|^2), \quad (4)$$

as discussed in Appendix A. As it is expected that  $\rho_\lambda$  is proportional to  $L$ , the mean and standard deviation can both be calculated to be proportional to  $1/\sqrt{L}$ . We therefore expect a phase transition in the distribution of  $|\lambda_{\min}|$  at  $t_c$  where the scaling behavior of  $\langle |\lambda_{\min}| \rangle$  as a function of  $L$  changes.

The distribution of  $\lambda_{\min}$  is plotted in Fig. 2(d) for the  $L = 500$  system around the critical time determined from the Loschmidt zeros. Indeed, we see the smallest eigenvalues reaching zero at  $t \approx 1.1$  and the distribution undergoing a qualitative transition to a form that closely follows the Rayleigh distribution above critical times. That this is indeed a phase transition is demonstrated in Fig. 3 for two different quenches. In Figs. 3(a) and 3(c) we plot  $\langle |\lambda_{\min}| \rangle$  and  $\sigma(|\lambda_{\min}|)\sqrt{L}$  for the quench of the microscopic model also considered in Fig. 1. We observe a plateau in  $\langle |\lambda_{\min}| \rangle$  for  $t \gtrsim t_c \approx 4.6$  consistently with the appearance of the Loschmidt zeros in Fig. 1. We have verified that  $\langle |\lambda_{\min}| \rangle$  scales as  $1/\sqrt{L}$  in the large- $t$  region. A phase transition is also clearly signalled by the jump in  $\sigma(|\lambda_{\min}|)\sqrt{L}$  observed at  $t = t_c$ . The apparent convergence of the curve for  $\sigma(|\lambda_{\min}|)\sqrt{L}$  indicates that the standard deviation scales as  $1/\sqrt{L}$  for all times. This confirms that the eigenvalue distribution of  $M(t)$  converges to a region with a well-defined boundary.

Figures 3(b) and 3(d) show the corresponding data for a quench starting from the ground state of model 3 with  $h = 0, J = 1$  and quenching to  $h = 5, J = 1$ . The behavior of

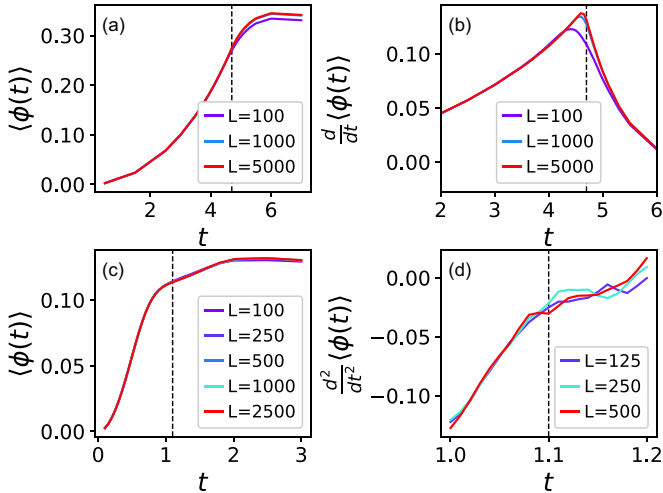


FIG. 4. Disorder averaged rate function and its derivatives. Panels (a), (b) show the microscopic model introduced in Fig. 1 while panels (c), (d) show data for the ground state quench discussed in connection with Fig. 2. The number of disorder realizations for panels (a) and (b) is  $N = 10\,000$ ,  $N = 5\,000$  and  $N = 200$  for system sizes  $L = 100$ ,  $L = 1\,000$  and  $L = 5\,000$ , respectively. For panel (c) the number of disorder realizations is  $N = 1\,000$  for  $L = 100$ ,  $250$  and  $N = 10\,000$  for  $L = 500$  while for panel (d) we used  $NL = 2.5 \times 10^7$ .

$\langle |\lambda_{\min}| \rangle$  is similar with an initial decrease and a transition to a plateau where  $\langle |\lambda_{\min}| \rangle$  approaches zero with increasing  $L$ . The critical time can be estimated from the extrapolated data as  $t_c \approx 1.1$ . The main difference to the previous quench is that  $\sigma(|\lambda_{\min}|)$  decreases slower than  $1/\sqrt{L}$  for  $t < t_c$ , consistently with the “fuzzier” boundary of the eigenvalue distribution compared to Fig. 1. Still, the mean and the standard deviation scale to zero for  $t \gtrsim 1.1$ , indicating that  $|\lambda_{\min}| = 0$  for all realizations in the thermodynamic limit.

#### IV. RATE FUNCTION AND ORDER OF THE DYNAMICAL PHASE TRANSITIONS

Above we have discussed DQPTs based on the appearance of Loschmidt zeros at a certain critical time, and linked this phenomenon to the eigenvalue distribution of the Loschmidt matrix. Dynamical phase transitions are typically defined in terms of nonanalyticities in the rate function  $\phi(t) = \log(Z(t))/L$ , also dubbed the “dynamical free energy,” and the type of the zero-manifold is connected to the order of the phase transition. A 1D zero-manifold with a finite line-density of zeros leads to a first order jump in the dynamical free energy, while crossing into a 2D manifold with a sudden jump in the 2D density of zeros corresponds to a second order transition [11, 14].

In the case of disordered systems the rate function itself becomes a random variable. We have computed the mean of the rate function by sampling over a large number of disorder realizations. We can then compute derivatives of  $\langle \phi(t) \rangle$  using simple finite difference differentiation. In Figs. 4(a) and 4(b) we demonstrate the appearance of a second order phase transition in the quench of the microscopic model of Fig. 1, clearly signalled by a peak in the first derivative of the rate function

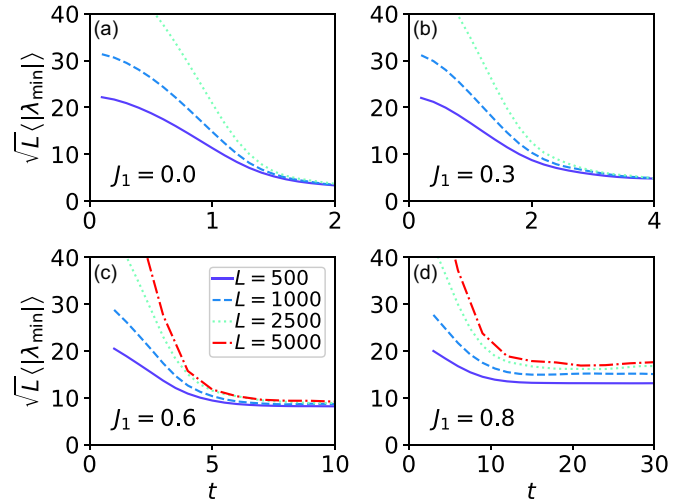


FIG. 5. Scaled mean of the distribution of  $|\lambda_{\min}|$  for quenches from the ground state of Hamiltonian 3. The system is quenched from  $J = J_0 = 1, h = 5$  to  $J = J_1, h = 5$  with the same random potential realization in the initial and final states. The panels show results for different  $J_1$ . Ensemble sizes are as in Fig. 3.

which becomes sharper with increasing system size. We have also checked that the density of eigenvalues of the Loschmidt matrix  $M(t)$  at the origin (not shown here) undergoes a transition where a jump from zero density to a finite density occurs and becomes increasingly sharp with increasing system size.

In Figs. 4(c) and 4(d) we present data for the ground state quench of Fig. 2. Here we may expect a higher order phase transition, as the eigenvalue density plotted in Fig. 2(c) does not develop a discontinuous jump. However, because the eigenvalues of  $M(t)$  close to zero are very sparse compared to the previous case, a much larger number of potential realizations is needed to gather good statistics. We suspect the transition is of order 3, but we cannot perform a proper finite size scaling analysis even with the extensive statistics used in Fig. 4(d). Thus, despite the rather sharp appearance of the Loschmidt zeros in Fig. 2, and the change in the scaling behavior of the smallest eigenvalue, we cannot conclusively identify the order of this DQPT, and the possibility even remains that it is a continuous crossover.

#### V. STRONG AND WEAK QUENCHES

It has been widely observed that a sudden quench through an equilibrium critical point typically results in rich dynamics and DQPTs [18], in contrast to quenches within one equilibrium phase. This property, though not without exceptions [19], has even been proposed as a diagnostic tool to investigate equilibrium phase boundaries. A remarkable feature of the transitions studied in this work is that they are not related to the Anderson localization transitions. The model (3) exhibits localization for any disorder strength  $h > 0$ , and one might wonder if the DQPT is related to quenching from  $h = 0$  to  $h > 0$  or vice versa. This is not the case, as demonstrated in Fig. 5. Here the quench is between two points in the parameter space where the system is deep in the localized phase. However, it is evident that the scaling of  $\langle |\lambda_{\min}| \rangle$  with  $\sqrt{L}$  is

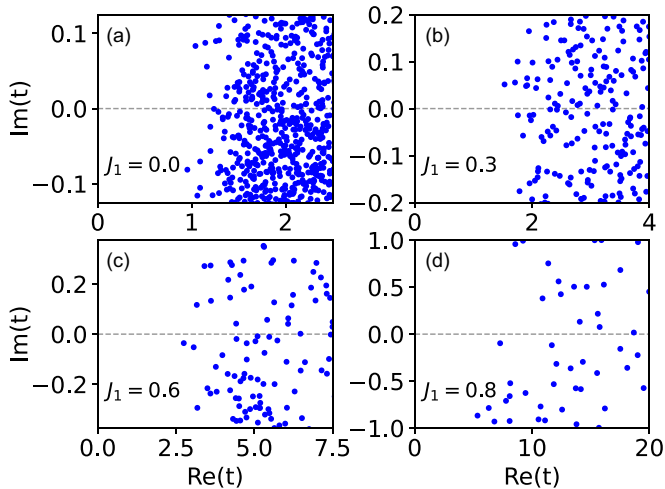


FIG. 6. Loschmidt zeros for an ensemble of  $N_s = 400$  systems of size  $L = 500$  for the same models as in Fig. 5.

different for early and late times, signifying an occurrence of a transition in the eigenvalue distribution. This transition is again associated with the appearance of Loschmidt zeros as demonstrated in Fig. 6.

We finally consider the difference between “weak” and “strong” quenches. If we let  $J_1$  approach  $J_0$ , the post-quench Hamiltonian approaches the initial Hamiltonian. If the system had a gapped ground state, we would expect that the ground states of  $H_1$  and  $H_0$  also approach each other, and that any possible dynamical phase transition would eventually disappear. However, since there is no gap in the thermodynamic limit, this argument is not applicable. In fact, it seems that the DQPT appears also for small quenches of  $J$  but reaching the scaling limit requires larger system sizes, as seen in Figs. 3(c) and 3(d). This is also seen in the Loschmidt zeros, whose density decreases when the quench becomes weaker. Thus, a larger system size or a larger ensemble of systems is required to characterize the zero-manifold.

## VI. DISCUSSION AND SUMMARY

In this work we developed the theory of Loschmidt echo in disordered noninteracting fermionic models after a quench. We showed that the Loschmidt zeros are best understood in terms of the eigenvalues of the Loschmidt matrix  $M(t)$  defined in Eq. (1), and we developed a scaling theory that links the discovered new type of singular many-body dynamics to phase transitions in the eigenvalue distribution of  $M(t)$ . Unexpectedly, we find that generic quenches lead to qualitatively similar DQPTs. Specifically, DQPTs appear also when performing quenches deep within the localized phase, which clearly rules out the idea that DQPTs could be employed to pinpoint the localization transition. A similar DQPT was also found in a generic GUE random matrix model, which points to a rather universal phenomenon independent of details such as dimension as long as disorder is present in the quench power spectrum.

Our findings constitute a radical departure from previous results in similar models. The bosonic Anderson model [20] and the fermionic Aubry-Andre model [21] were found to

exhibit periodic Loschmidt zeros when quenched through the localization transition point, but not when quenched within the localized or delocalized phase. However, the crucial difference is that Ref. [21] considers a single fermion and Ref. [20] considers many bosons in the same state, while we deal with generic fermionic Slater determinant states. Periodic dynamical phase transitions were also found in the many-body time evolution of the interacting Aubry-Andre model with system sizes up to  $L = 100$  [22]. It would be interesting to revisit the Aubry-Andre model using the eigenvalues of the  $M(t)$ -matrix and perform a scaling analysis to determine the type of the zero-manifolds as we have done here for the model with Anderson disorder.

DQPTs have also been found in Ising chains with disorder [23–26] even in quenches that do not cross the bulk localization transition [23]. This was attributed to crossing into a Griffiths phase [23], with the intuitive picture that parts of the system, the so-called rare regions, have effectively crossed over the phase transition point even if the bulk remains within the same phase. It was also found that the Loschmidt zeros can accumulate into areas instead of lines [23] in the thermodynamic limit, which resembles the findings in our work. The transverse field Ising model and its extensions considered in Refs. [23–26] can be mapped to free fermions via the Jordan-Wigner transformation, although the resulting Hamiltonians do not conserve particle number and there is no direct correspondence to the models we have considered. Nevertheless, it would be interesting to study if, e.g., the rare regions might play a part also in the DQPTs we have discussed. Another point of view is that, besides being the essential cause of DQPTs, disorder can modify singular dynamics appearing in clean models, such as in the Kitaev chain [27].

Finally, the methodology developed in our work can be useful for treating many noninteracting fermionic models without translation invariance. Considering the eigenvalues of  $M(t)$  is complementary to the recently developed cumulant method [15,28] which has been applied to strongly correlated systems in 1D and 2D. In the present work we also developed a variant of the cumulant method to efficiently study large noninteracting but disordered models. We expect these ideas to stimulate further studies of the dynamics of disordered systems.

## ACKNOWLEDGMENTS

The authors acknowledge the Academy of Finland Project No. 331094 for support. Computing resources were provided by CSC—the Finnish IT Center for Science. The QuSpin package [29,30] was employed in the calculations.

## APPENDIX A: EXPECTED DISTRIBUTION OF MINIMAL EIGENVALUE

To model the distribution of the minimal eigenvalue of the matrix  $M(t)$  for  $t > t_c$ , we consider a small circle of radius  $R$  around the origin and assume that the eigenvalues within this circle are independently and uniformly distributed with density  $\rho_\lambda$ . The number of eigenvalues within the circle is thus  $N = \pi R^2 \rho_\lambda$ . The probability that all points are outside

a smaller circle of radius  $r$  is

$$P(|\lambda_{\min}| > r) = (1 - r^2/R^2)^N. \quad (\text{A1})$$

The cumulative distribution function for the scaled variable  $|\lambda_{\min}|/\sqrt{\rho_\lambda}$  is then

$$\begin{aligned} F(x) &= P(|\lambda_{\min}|/\sqrt{\rho_\lambda} < x) \\ &= P(|\lambda_{\min}| < x/\sqrt{\rho_\lambda}) = 1 - P(|\lambda_{\min}| > x/\sqrt{\rho_\lambda}) \\ &= 1 - \left(1 - \frac{\pi x^2}{\pi \rho_\lambda R^2}\right)^N = 1 - \left(1 - \frac{\pi x^2}{N}\right)^N. \end{aligned} \quad (\text{A2})$$

When the system size grows, we expect  $\rho_\lambda \rightarrow \infty$  so that  $N \rightarrow \infty$ . The cumulative function then converges to

$$F(x) \rightarrow 1 - \exp(-\pi x^2). \quad (\text{A3})$$

The cumulative function of the Rayleigh distribution is usually written as

$$F_{\text{Rayleigh}}(x) = 1 - \exp(-x^2/(2\sigma^2)), \quad (\text{A4})$$

where  $\sigma$  is a scale parameter. Thus,  $|\lambda_{\min}|/\sqrt{\rho_\lambda}$  becomes Rayleigh distributed with scale parameter  $\sigma = 1/\sqrt{2\pi}$ , while the distribution of  $|\lambda_{\min}|$  becomes increasingly narrow as  $\rho_\lambda$  increases, and can be approximated by a Rayleigh distribution with the scale parameter  $\sigma = 1/\sqrt{2\pi\rho_\lambda}$ .

## APPENDIX B: SPECIALIZATION OF THE CUMULANT METHOD FOR NON-INTERACTING SYSTEMS

The cumulant method developed in Ref. [15] can be used to locate the Loschmidt zeros in the complex plane. In principle the method can be directly applied also to the noninteracting models discussed in this work. However, specializing the computation of the cumulants to the case of Slater determinant states naturally offers a huge numerical advantage, because it avoids handling general many-body state vectors.

The Loschmidt echo as a function of the imaginary time  $\tau$  can be defined as

$$Z(\tau) = \langle \Psi | \exp(-\tau H_1) | \Psi \rangle, \quad (\text{B1})$$

where  $H_1$  is the post-quench Hamiltonian and  $|\Psi\rangle$  is taken to be some eigenstate of the prequench Hamiltonian  $H_0$ . If  $H_0$  is a noninteracting fermionic Hamiltonian, then the state  $|\Psi\rangle$  is a Slater determinant of single-particle states. We collect the states to a tall matrix  $V$  so that each column is a single-particle eigenstate. If we also assume that  $H_1$  is noninteracting, then the state  $|\Psi(\tau)\rangle = \exp(-\tau H_1) |\Psi\rangle$  is also always a Slater determinant where the single-particle states are time-developed by  $H_1$ . Thus,  $|\Psi(\tau)\rangle$  is represented by the time-developed tall matrix  $V(\tau) = \exp(-\tau H_1)V$ .

The overlap of Slater determinants is given by the determinant of the overlap matrix [13],

$$Z(\tau) = \det(V^\dagger V(\tau)). \quad (\text{B2})$$

In the interacting case [15] the cumulants are calculated from the moments

$$\mu_n = \partial_\tau^n Z(\tau). \quad (\text{B3})$$

However, the first derivative of the determinant of a matrix  $M(\tau) = V^\dagger V(\tau)$  is

$$\partial_\tau \det(M(\tau)) = \det(M(\tau)) \text{tr}(M(\tau)^{-1} \partial_\tau M(\tau)), \quad (\text{B4})$$

with successively more complicated formulas for higher derivatives. It is thus difficult to directly compute the moments as derivatives of the  $Z$ .

For the Slater determinant case we can instead start from the formula for the cumulants

$$\kappa_n = \partial_\tau^n \log(\det(M(\tau)))|_{\tau=\tau_0}, \quad (\text{B5})$$

which for  $n = 1$  becomes

$$\kappa_1 = \text{tr}(M(\tau)^{-1} \partial_\tau M(\tau))|_{\tau=\tau_0}. \quad (\text{B6})$$

Let us then define a matrix function  $K'(\tau)$  such that

$$K'(\tau) = M(\tau)^{-1} \partial_\tau M(\tau), \quad (\text{B7})$$

or equivalently

$$\partial_\tau M(\tau) = M(\tau) K'(\tau). \quad (\text{B8})$$

We then have that  $\kappa_n = \text{tr}(\partial_\tau^{n-1} K'(\tau))|_{\tau=\tau_0}$ .

In the case of a single particle  $M$  would be a  $1 \times 1$  matrix and we could just define  $K(\tau) = \log(M(\tau)) = \log(Z(\tau))$  and  $K'(\tau) = \partial_\tau K(\tau)$ .  $K$  and  $M$  would then just be the cumulant and moment generating functions. However, we do not want to do so because the derivative of the matrix logarithm is again nontrivial, and we do not actually need to define  $K(\tau)$ . It is enough to have a well-defined  $K'(\tau)$  which is not necessarily a derivative of a known function  $K(\tau)$ .

Now we can proceed as in the usual case to derive a formula that relates cumulants to moments. But now our moments and cumulants are matrices,

$$K'(\tau) = \sum_{n=1}^{\infty} K_n \frac{(\tau - \tau_0)^{n-1}}{(n-1)!} \quad (\text{B9})$$

and

$$M(\tau) = \sum_{n=0}^{\infty} M_n \frac{(\tau - \tau_0)^n}{n!}. \quad (\text{B10})$$

Equating the coefficient of  $\tau^{n-1}$  on both sides of Eq. (B8) we get

$$\begin{aligned} \frac{M_n}{(n-1)!} &= \sum_{k=1}^n M_{n-k} K_k \frac{1}{(k-1)!(n-k)!} \\ &= \frac{M_0 K_n}{(n-1)!} + \sum_{k=1}^{n-1} M_{n-k} K_k \frac{1}{(k-1)!(n-k)!}, \end{aligned} \quad (\text{B11})$$

which can be solved for  $K_n$  as

$$\begin{aligned} K_n &= M_0^{-1} \left[ M_n - \sum_{k=1}^{n-1} M_{n-k} K_k \frac{(n-1)!}{(k-1)!(n-k)!} \right] \\ &= M_0^{-1} \left[ M_n - \sum_{k=1}^{n-1} \binom{n-1}{k-1} M_{n-k} K_k \right]. \end{aligned} \quad (\text{B12})$$

For the  $1 \times 1$  case this again just reduces to the usual recursive formula for the cumulants in terms of the moments. In

fact, it is the same formula, but it has to be remembered that the matrices do not necessarily commute.

Numerically, we first compute the moment matrices  $M_n = V^\dagger \partial_\tau^n V(\tau)|_{\tau=\tau_0}$ , and then use the recursive formula to get

the cumulant matrices  $K_n$ . The cumulants  $\kappa_n$  are then found as the trace of the matrices  $K_n$ . Finding the zeros using the cumulants proceeds as in the interacting case [15].

- 
- [1] T. Tian, H.-X. Yang, L.-Y. Qiu, H.-Y. Liang, Y.-B. Yang, Y. Xu, and L.-M. Duan, Observation of Dynamical Quantum Phase Transitions with Correspondence in an Excited State Phase Diagram, *Phys. Rev. Lett.* **124**, 043001 (2020).
- [2] K. Xu, Z.-H. Sun, W. Liu, Y.-R. Zhang, H. Li, H. Dong, W. Ren, P. Zhang, F. Nori, D. Zheng, H. Fan, and H. Wang, Probing dynamical phase transitions with a superconducting quantum simulator, *Sci. Adv.* **6**, eaba4935 (2020).
- [3] A. Eckardt, Colloquium: Atomic quantum gases in periodically driven optical lattices, *Rev. Mod. Phys.* **89**, 011004 (2017).
- [4] N. Fläschner, D. Vogel, M. Tarnowski, B. S. Rem, D.-S. Lühmann, M. Heyl, J. C. Budich, L. Mathey, K. Sengstock, and C. Weitenberg, Observation of dynamical vortices after quenches in a system with topology, *Nat. Phys.* **14**, 265 (2018).
- [5] T. Fogarty, S. Deffner, T. Busch, and S. Campbell, Orthogonality Catastrophe as a Consequence of the Quantum Speed Limit, *Phys. Rev. Lett.* **124**, 110601 (2020).
- [6] X.-Y. Guo, C. Yang, Y. Zeng, Y. Peng, H.-K. Li, H. Deng, Y.-R. Jin, S. Chen, D. Zheng, and H. Fan, Observation of a Dynamical Quantum Phase Transition by a Superconducting Qubit Simulation, *Phys. Rev. Appl.* **11**, 044080 (2019).
- [7] T. Tian, Y. Ke, L. Zhang, S. Lin, Z. Shi, P. Huang, C. Lee, and J. Du, Observation of dynamical phase transitions in a topological nanomechanical system, *Phys. Rev. B* **100**, 024310 (2019).
- [8] K. Wang, X. Qiu, L. Xiao, X. Zhan, Z. Bian, W. Yi, and P. Xue, Simulating Dynamic Quantum Phase Transitions in Photonic Quantum Walks, *Phys. Rev. Lett.* **122**, 020501 (2019).
- [9] J. Zhang, G. Pagano, P. W. Hess, A. Kyprianidis, P. Becker, H. Kaplan, A. V. Gorshkov, Z.-X. Gong, and C. Monroe, Observation of a many-body dynamical phase transition with a 53-qubit quantum simulator, *Nature (London)* **551**, 601 (2017).
- [10] P. Jurcevic, H. Shen, P. Hauke, C. Maier, T. Brydges, C. Hempel, B. P. Lanyon, M. Heyl, R. Blatt, and C. F. Roos, Direct Observation of Dynamical Quantum Phase Transitions in an Interacting Many-Body System, *Phys. Rev. Lett.* **119**, 080501 (2017).
- [11] M. Heyl, Dynamical quantum phase transitions: A review, *Rep. Prog. Phys.* **81**, 054001 (2018).
- [12] M. Heyl, Scaling and Universality at Dynamical Quantum Phase Transitions, *Phys. Rev. Lett.* **115**, 140602 (2015).
- [13] F. Plasser, M. Ruckebauer, S. Mai, M. Oppel, P. Marquetand, and L. González, Efficient and flexible computation of many-electron wave function overlaps, *J. Chem. Theory Comput.* **12**, 1207 (2016).
- [14] M. Schmitt and S. Kehrein, Dynamical quantum phase transitions in the Kitaev honeycomb model, *Phys. Rev. B* **92**, 075114 (2015).
- [15] S. Peotta, F. Brange, A. Deger, T. Ojanen, and C. Flindt, Determination of Dynamical Quantum Phase Transitions in Strongly Correlated Many-Body Systems Using Loschmidt Cumulants, *Phys. Rev. X* **11**, 041018 (2021).
- [16] T. Tao and V. Vu, Random matrices: The distribution of the smallest singular values, *Geom. Funct. Anal.* **20**, 260 (2010).
- [17] F. Benaych-Georges and R. R. Nadakuditi, The singular values and vectors of low rank perturbations of large rectangular random matrices, *J. Multivariate Anal.* **111**, 120 (2012).
- [18] A. Haldar, K. Mallayya, M. Heyl, F. Pollmann, M. Rigol, and A. Das, Signatures of Quantum Phase Transitions after Quenches in Quantum Chaotic One-Dimensional Systems, *Phys. Rev. X* **11**, 031062 (2021).
- [19] S. Vajna and B. Dóra, Disentangling dynamical phase transitions from equilibrium phase transitions, *Phys. Rev. B* **89**, 161105(R) (2014).
- [20] H. Yin, S. Chen, X. Gao, and P. Wang, Zeros of Loschmidt echo in the presence of anderson localization, *Phys. Rev. A* **97**, 033624 (2018).
- [21] C. Yang, Y. Wang, P. Wang, X. Gao, and S. Chen, Dynamical signature of localization-delocalization transition in a one-dimensional incommensurate lattice, *Phys. Rev. B* **95**, 184201 (2017).
- [22] R. Modak and D. Rakshit, Many-body dynamical phase transition in a quasiperiodic potential, *Phys. Rev. B* **103**, 224310 (2021).
- [23] J. A. Hoyos, R. F. P. Costa, and J. C. Xavier, Disorder-induced dynamical Griffiths singularities after certain quantum quenches, *Phys. Rev. B* **106**, L140201 (2022).
- [24] D. Trapin, J. C. Halimeh, and M. Heyl, Unconventional critical exponents at dynamical quantum phase transitions in a random Ising chain, *Phys. Rev. B* **104**, 115159 (2021).
- [25] J. C. Halimeh, N. Yegovtsev, and V. Gurarie, Dynamical quantum phase transitions in many-body localized systems, [arXiv:1903.03109](https://arxiv.org/abs/1903.03109) (2019).
- [26] V. Gurarie, Dynamical quantum phase transitions in the random field Ising model, *Phys. Rev. A* **100**, 031601(R) (2019).
- [27] U. Mishra, R. Jafari, and A. Akbari, Disordered Kitaev chain with long-range pairing: Loschmidt echo revivals and dynamical phase transitions, *J. Phys. A: Math. Theor.* **53**, 375301 (2020).
- [28] F. Brange, S. Peotta, C. Flindt, and T. Ojanen, Dynamical quantum phase transitions in strongly correlated two-dimensional spin lattices following a quench, *Phys. Rev. Res.* **4**, 033032 (2022).
- [29] P. Weinberg and M. Bukov, QuSpin: A Python package for dynamics and exact diagonalisation of quantum many body systems. Part I: Spin chains, *SciPost Phys.* **2**, 003 (2017).
- [30] P. Weinberg and M. Bukov, QuSpin: A Python package for dynamics and exact diagonalisation of quantum many body systems. Part II: Bosons, fermions, and higher spins, *SciPost Phys.* **7**, 020 (2019).